

Journal of Materials Chemistry A

Accepted Manuscript



This is an *Accepted Manuscript*, which has been through the Royal Society of Chemistry peer review process and has been accepted for publication.

Accepted Manuscripts are published online shortly after acceptance, before technical editing, formatting and proof reading. Using this free service, authors can make their results available to the community, in citable form, before we publish the edited article. We will replace this *Accepted Manuscript* with the edited and formatted *Advance Article* as soon as it is available.

You can find more information about *Accepted Manuscripts* in the [Information for Authors](#).

Please note that technical editing may introduce minor changes to the text and/or graphics, which may alter content. The journal's standard [Terms & Conditions](#) and the [Ethical guidelines](#) still apply. In no event shall the Royal Society of Chemistry be held responsible for any errors or omissions in this *Accepted Manuscript* or any consequences arising from the use of any information it contains.

ARTICLE

Ultra high-yield one-step synthesis of conductive, and superhydrophobic three-dimensional mats of carbon nanofibers via full catalysis of unconstrained thin film

Cite this: DOI: 10.1039/x0xx00000x

Received 00th January 2012,
Accepted 00th January 2012

DOI: 10.1039/x0xx00000x

www.rsc.org/

Efrat Shawat¹, Ilana Perelshtein¹, Andrew Westover², Cary L. Pint², and Gilbert D. Nessim^{1}*

1. Department of Chemistry, Bar Ilan Institute for Nanotechnology and Advanced materials (BINA), Bar Ilan University, Ramat Gan, 52900, Israel
2. Department of Mechanical Engineering, Vanderbilt University, Nashville, TN 37235, USA

We directly synthesized large conductive and superhydrophobic three-dimensional mats of entangled carbon nanofibers (CNFs) using thermal chemical vapor deposition (CVD). We show that the yield obtained from the catalysis of an unconstrained thin Ni-Pd film is over an order of magnitude higher compared to the same thin film when bound to a substrate. The growth mechanism differs from substrate-bound growth, where catalysis occurs only the top surface of the catalytic film, as the full Ni-Pd catalyst layer participates in the reaction and is totally consumed to bi-directionally grow CNFs. Therefore, the yield further increased with the thin film thickness, in contrast with substrate-bound growth. The unconstrained growth occurred thanks to a weak adhesion layer that delaminated during the thermal process. Additionally, we showed that the supporting substrate material strongly affected the nanostructure morphology obtained. The as-grown CNF mats were used as a three-dimensional electrode for lithium-ion batteries. We envisage these CNF mats to be an ideal platform to be functionalized for multiple applications including high-performance electrodes, sensors, electromagnetic shields, and conductive polymer-coated composites.

Introduction

Carbon nanofibers (CNFs)¹⁻³ are a class of carbon nanostructure that exhibit interesting mechanical,^{4, 5} electrical⁶

and thermal⁷ properties relevant for various applications. CNFs have gained significant attention due their synthetic processes that require less precision and energy input compared to other carbon nanostructures,³ such as carbon nanotubes.⁸ Synthesis processes for CNFs² typically involve the decomposition of

gas-phase hydrocarbons over metal catalyst particles (e.g. Fe⁹, Co,^{10, 11} Ni, and alloys), which leads to saturation of the metal catalyst with carbon and subsequent precipitation of CNFs.^{2, 12} Studies have emphasized the crucial role that catalyst support materials play in this process, dictating the energetics governing the catalytic activity of the particles as well as the physical mode for CNF growth (e.g. tip-growth or base-growth).^{12, 13, 14} Additionally, the growth of CNFs from bulk-like metal alloy layers have indicated novel growth mechanisms where fragmenting of the metallic surface layer due to carbon interaction enables simultaneous tip-growth and base-growth modes from the same catalyst particles.¹⁵ This research emphasizes the importance of the architecture involving the catalyst and underlayer materials in dictating the growth mechanism and behavior, which is a concept that could be extended to growth processes operating in a similar manner and involving both single- and multi-walled carbon nanotubes^{16, 17}

A key challenge for synthetic techniques is the ability to build upon growth mechanisms to engineer catalyst architectures that enable hierarchical assemblies of nanostructures into templates directly usable in applications.¹⁸ These assembly routes dictate the feasibility of such materials for use in applications spanning across energy storage, energy conversion, catalysis, among other areas, where the device performance is strongly correlated to how such nanostructures are assembled.^{19, 20} Whereas previous studies have emphasized the ability to posthumously control assembly of CNF¹⁹ or CNT²¹ materials directly grown on supporting substrates, to adapt such materials in lithium-ion batteries, the presence of a supporting substrate often hinders applicability. Nonetheless, CNFs and CNTs have been demonstrated as excellent anode template materials for lithium-ion batteries building upon commercially implemented anode-electrolyte-cathode chemistries, but with promise of higher rate capability and in some cases better storage capacity.^{6, 22, 23, 24, 25, 26}

In this research, we demonstrate synthesis control of freestanding, three-dimensional, super-hydrophobic, conductive mats of CNFs via controlled self-delamination of the catalytic stack. We show that all the catalytic material participates in a bi-directional growth mechanism and not only its top surface as occurs in substrate-bound growth. This leads to yields over an order of magnitude compared to substrate-bound growth. Additionally, we show how the delamination process can be modulated by the choice of the substrate to dramatically affect the morphology of the carbon nanostructures. Finally, we demonstrate how the freestanding foam-like CNF mat obtained yields storage capacities for lithium-ion batteries comparable to bulk carbon anodes for volumetrically thick structures.

Experimental section

Carbon nanofiber (CNF) growth was performed on clean, polished n-type Si (100) wafers using thin films of Ni (5 nm) over Pd (200 nm) with Ti adhesion layer deposited by e-beam evaporation without breaking vacuum at a pressure of 1×10^{-6} Torr. The wafers were manually cleaved into 5×5 mm samples using a diamond scribe. Catalyst pretreatment followed by CNT growth was performed in two atmospheric-pressure furnaces (Lindberg Blue) connected in series, in a single fused-silica tube with an internal diameter of 22 mm. The first furnace preheated the source gases (at 770 °C), while the sample was positioned in the second furnace for the annealing and growth steps (650 °C). The furnace temperatures were displayed by the

built-in furnace thermocouples. Flows of Ar (99.999%), Ar/O₂ (mixture of 99% Ar with 1% oxygen), C₂H₄ (99.5%), and H₂ (99.999%) were maintained using electronic mass flow controllers (MKS 247D). All experiments were performed using the “fast-heat” technique, in which the samples were initially positioned outside the heated zone of the furnace with a fan blowing on the exposed quartz tube wall to keep them at room temperature. Argon and hydrogen flows of 100 and 400 standard cubic centimeters per minute (sccm), respectively, were maintained, while the two furnaces were ramped to the desired temperature. The flow rates of the gases remained constant in all studies at 100 sccm (Ar), 500 sccm (Ar/O₂), 400 sccm (H₂), and 300 sccm (C₂H₄) during growth. The CNTs were characterized by field-emission SEM (FESEM; FEI, Helios 600) operating at 5 keV and by high-resolution transmission electron microscopy (HRTEM) using a JEOL-2100 operating at 200 keV equipped with EDAX. HRTEM samples were prepared by dispersing a section of the CNF mats in 2-propanol with gentle sonication for an hour and then placing 1 drop of the solution on a 300 mesh Cu holey carbon grid (from SPI). XRD was used to determine the structure of the Pd and Ni catalysts. Finally, an analytical balance was used to weight the nanocarbon mat. We used a Ramé-Hart model 100 for contact angle measurement. Raman spectra were measured in a dual laser confocal (X100), LabRam HR using an excitation wavelength of 532 nm.

Results

CNF mats were synthesized using chemical vapor deposition in Ar/O₂ (a mixture of Ar and 1% O₂)^{1, 27}, H₂, and C₂H₄ gas mixtures on substrates with Ni / Pd catalyst layers (10 nm/200 nm, respectively) e-beam deposited on Ti/Si or Ti/SiO₂ substrates where the Ti adhesion layer ranged from 5 to 15 nm in thickness. The synthesis adopts techniques we previously developed such as fast heat, gas precursor preheating^{4, 6, 28-30}, and in-situ controlled formation of water vapor^{1, 27}. The Ti adhesion layer is necessary due to the poor adhesion of Pd to the Si or SiO₂ wafer^{6, 15}. For thick layers of Ti (15 nm), we synthesized entangled, micron-tall, CNFs on the substrate. For thin Ti layers (5 nm), we obtained three-dimensional CNF mats, separated from the substrate, with surface up to four times that of the substrate from which it originated (Fig. 1) and with weight up to 30 times what we obtained with the thick Ti layer (up to 35 mg/cm² compared to approximately 1 mg/cm², (Fig. 5 and Fig. S3). High-resolution transmission electron microscope (HRTEM) images of the CNFs from the delamination-enabled mats show the catalytic bidirectional growth of CNFs with embedded catalysts and diameters ranging from 70-160 nm with an average of 105 nm and standard deviation of 23 nm ((Fig. 1 (a2), and Fig. 4 in S.I.). Using a four-point probe, we measured the sheet resistance of the CNF mats to be approximately 200 Ω/□. Contact angle measurement show that the CNF mats are superhydrophobic with a contact angle of 157° (see Figure 5 in S.I.). Using Raman, we measured a G/D ratio of 0.9 (= 438 / 500), confirming the amorphous nature of the CNFs.

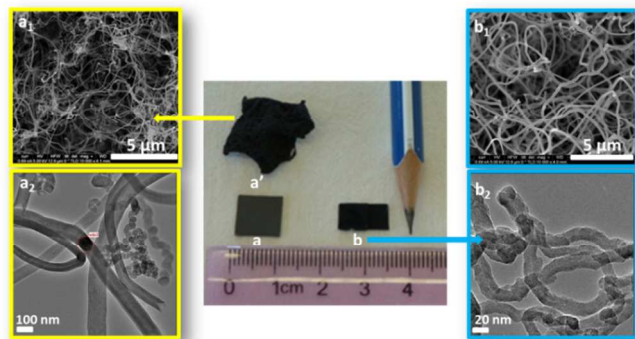


Fig. 1 Photo of mats (a') delaminated from substrate (a) and of substrate-bound CNFs (b). The delaminated mats are made of entangled CNFs (a₁) with catalytic bidirectional growth (a₂). The substrate-bound formation is also made of entangled CNFs (b₁) but no catalytic bidirectional growth is observed (b₂).

To pinpoint the transition from substrate-bound CNF mats to freestanding CNF mats, we performed experiments where we varied the Ti layer thickness between 5 to 15 nm (with Ni/Pd = 10/200 nm). For a Ti thickness 5 nm, we observed total delamination. X-ray diffraction (XRD) of the substrate from which the CNF mat delaminated indicated that no Ti was present on the Si substrate, while XRD of the CNF mat itself showed a small amount of Ti was detected as Ni₃Ti (Fig. S1). Although EDAX of the CNF catalyst did not detect Ti, given the small amount of Ti used, it is possible that it was below the detection limit. For a Ti thickness of 15 nm the CNF growth was substrate-bound while we observed partial delamination for a Ti thickness of 10 nm.

To understand the role of the Pd underlayer in the growth of freestanding CNF mats, we tested increasing Pd thicknesses (50, 100, and 200 nm). We observed that the yield of the freestanding mats significantly increased with the thickness of the Pd layer (Fig. 2). This shows that (a) Pd is indeed involved in the catalysis (most underlayers do not actively participate in CNT/CNF growth) and (b) that all the catalytic material (here an alloy of Ni/Pd, and possibly Ti) participated in the catalysis, and not just the top surface (as usually occurs in substrate-bound CNT/CNF growth).

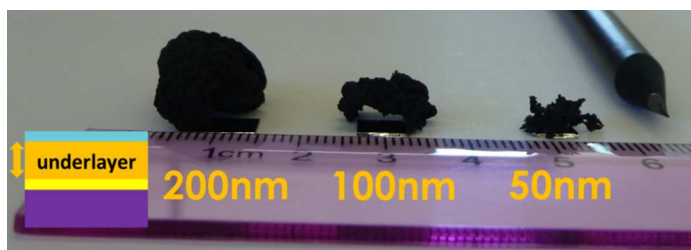


Fig. 2 Photo of mats delaminated from substrate grown with Pd layers of various thickness. The yield significantly increased for increasing thickness of the Pd underlayer.

Discussion

When delamination occurs, the CNF mats grow much larger than the growth substrate from which they delaminated, indicating that the mechanism for high-yield unconstrained growth is clearly different than that for low-yield substrate-bound growth. The catalyst embedded in the CNFs (Fig. 1a₂) is consistent with previously observed bi-directional growth using Ni and Pd catalyst layer^{6, 15}. In line with the mechanism previously described for bidirectional growth of CNFs, where catalyst particles formed by fragmentation occurring through carbon diffusion along grain boundaries¹⁵, we hypothesize that here all the Ni-Pd metal stack is catalytically active. Under growth conditions that yield substrate-bound mats (i.e., for thick Ti layers), the fragmentation at the grain boundaries of the top catalytic metal particles leads to a process where both mechanical coupling of the mat to a constrained substrate and diffusion limitations of the precursor lead to a slow growth from the ongoing fragmentation of catalysts (grains) during the growth process. In contrast, when delamination occurs (i.e., for thin Ti layers), we hypothesize that the release of the mechano-chemical constraints that limit the catalytic activity for substrate-bound growth, enable a faster fragmentation of metal catalysts and enhance diffusion of the carbon precursor to catalyze freestanding mats. Based on the extensive characterizations on our materials following partial and total delamination (HRSEM, HRTEM, elemental X-ray analysis (EDX), and x-ray diffraction (XRD)), we postulate the following mechanism (Fig. 3).

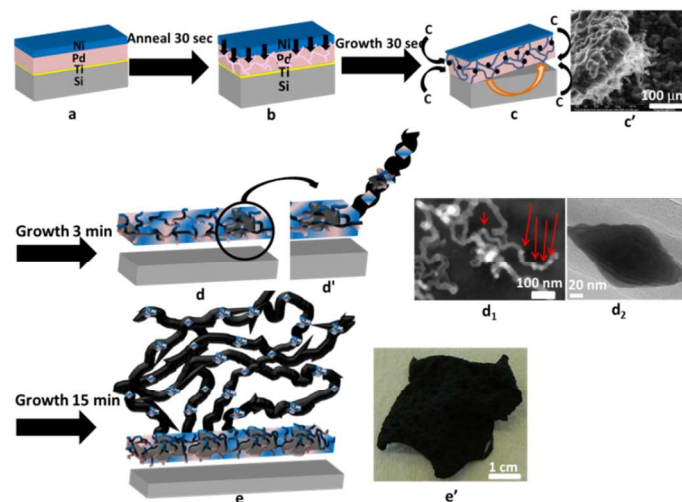


Fig. 3 Schematics with HRSEM and HRTEM images describing the proposed mechanism for delamination, nucleation, and growth. The details are described in the text.

During the initial short (30 seconds) reducing anneal step (Fig. 3b), we expect the Ni to start diffusing through the Pd grain boundaries¹⁵. The mechanism we propose for the delamination mediated by the thin Ti layer is based on the volumetric change in the Pd metal film associated with the inward diffusion of carbon species generating strain at the substrate interface (Fig. 3c). We hypothesize that the carbon species cause the strain by diffusing through the Pd grain boundaries and interstitially into the octahedral site of the face-centered cubic Pd lattice³¹. The C atoms diffusing in the Pd grain boundaries and lattice could also participate during the catalysis of the CNFs. It is important

to note that we did not observe delamination during annealing experiments where we did not flow the carbon precursor (not shown), thus confirming that the carbon precursor is critical to induce delamination.

Now that the catalytic thin layer is no longer constrained by the substrate, film stresses are removed and a larger catalytic surface is exposed to the incoming precursor gases, with likely acceleration of carbon diffusion through the grain boundaries of the thin catalytic film¹⁵. Consistently with the mechanisms discussed in our previous study using similar but substrate-bound Ni/Pd catalytic films, and supported by EDAX characterizations of our catalysts embedded in the CNFs, we also anticipate possible diffusion of Ni, and possibly Ti, through the Pd grain boundaries and to continue alloying with Pd to form a binary Ni-Pd alloy, or possibly a ternary Pd-Ni-Ti alloy³². When thick Ti interlayers are used, the robust adhesion at the Si-Ti and Pd-Ti interfaces overcomes the film strain and maintains substrate-bound CNF growth.

After 30 seconds, we observed partial delamination of the catalytic layer (Fig. 3c'), which exhibited very short growth. Following delamination, we observed the growth of CNFs from particles fragmented from pieces of the delaminated Ni-Pd-Ti films (Fig. 3c). XRD and EDAX of the CNF mats and of the catalysts embedded in the CNFs, emphasize the presence of Ni, Pd, and Ti in the mats with no observed presence of any metal left on the Si substrate after delamination (Fig. S2); this analysis confirms that the delamination occurs at the Ti-Si interface, and that the resulting metal films nucleate and evolve into the unconstrained, freestanding materials observed after delamination occurs. Similarly to the fragmentation-based mechanism we observed in our previous study¹⁵, we believe that each initial grain of Pd, which now has alloyed with Ni, and possibly Ti, is bi-directionally growing CNFs (Fig. 3d, d', d1, and d2). Since more surfaces are now exposed and the mechanical constraint from the substrate has been removed, all catalyst grains can now participate in the catalysis and bi-directionally grow CNFs, thus maximizing the yield. The large network of entangled CNFs obtained after 15 minutes of growth results in the formation of freestanding CNF mats (Fig. 3e and 3e').

Since the delamination process is the key of our synthesis to yield large freestanding CNF mats, we wondered if by changing the substrate, we could sufficiently affect the delamination process to yield different nanostructures. When we used Si wafers coated with thermal SiO₂, instead of the pristine Si wafers used in our study, we again observed a high yield of carbon nanostructures but with a uniquely different morphology (Fig. 4). The CNFs obtained following delamination from SiO₂ substrates are composed of hair-like or stranded features (Fig. 4b) in comparison to the smoother macroscopic morphological properties of the mat obtained following delamination from Si substrates (Fig. 4a).

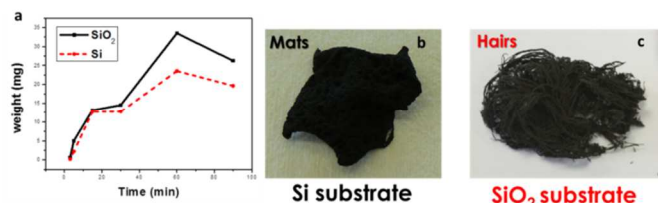


Figure 4. CNF mats obtained from Si substrates (a) and from SiO₂ substrates (b). The yield obtained from SiO₂ substrates is highly higher for any growth duration (c).

We also noticed that the yield obtained using SiO₂ as a substrate was slightly higher for any growth duration (Fig. 4c; images of the mats and hairs obtained are shown in Fig. S3). As we emphasize that the key interface associated with delamination of the Ni-Pd catalyst layer is the interface between the Ti adhesion layer and the substrate, this confirms that varying the substrate material can lead to controllable modification of the three-dimensional carbon nanostructure morphology based on the manner in which the catalyst film delaminates from the substrate. This underlines a level of controllability in the macroscopic mat properties that can be uniquely modified based upon the substrate-adhesion layer interaction that mediates delamination.

Application example: as-is synthesized CNF mat as Li-ion anode

A key challenge in developing applications from CNFs or CNTs requires the assembly of these materials into functional templates usable in devices. The one-step synthesis presented here is attractive as we can readily obtain a nanostructure that can serve as platform to be functionalized for various applications. The porous three-dimensional nature of the conductive CNF mats synthesized could be functionalized with active material to fabricate efficient electrodes for batteries⁴. As an illustration, we tested the as-grown CNF mats as anodes for Li-ion batteries. This would provide a baseline from which the anode could be improved through additional functionalization.

Compared to the utilization of conventional micron-scale graphitic anodes, the use of freestanding CNFs enables capability to use millimeter-scale thickness anode materials while leaving accessible surface of active material compatible with routes to develop advanced cathodes or anodes for batteries³³. Freestanding 3-D electrodes minimize the packaging needed for commercially-employed electrodes that must be utilized in thin film electrodes. Similarly, we used CNF mats as anodes in half-cell lithium-ion battery configurations by utilizing 1 M LiPF₆ electrolytes dissolved in ethylene carbonate – dimethyl carbonate solvents. Millimeter-scale thickness CNF mats were pressed into coin cells, and then subjected to galvanostatic and cyclic voltammetry (CV) testing at voltages (vs. Li/Li⁺) of 2 V and less, corresponding to usable capacity in a full cell configuration (Fig. 5).

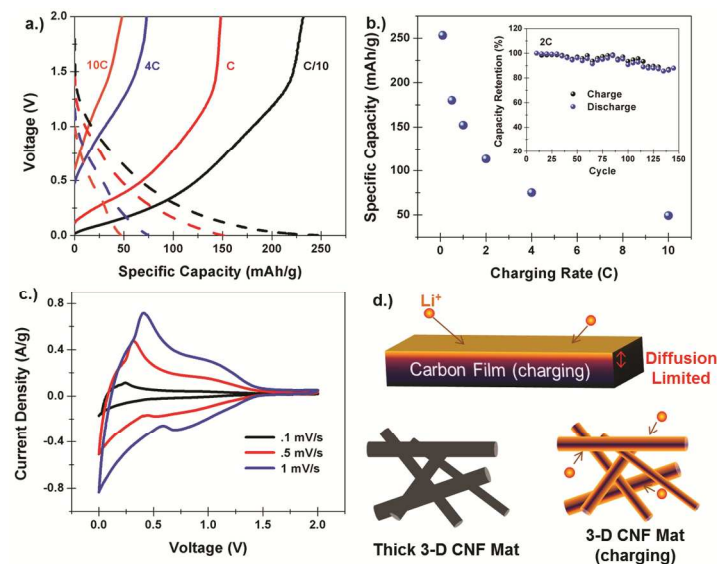


Fig. 5 (a) Galvanostatic charge-discharge cycling of freestanding 3-D CNF mats (vs. Li/Li^+), with discharge curves shown in dashed lines, (b) rate capability plot of capacity (at 2 V vs. Li/Li^+) vs. the rate of charging. Inset is a plot of capacity retention at 2 C for 150 cycles. (c) Cyclic voltammetry from 0.1 – 1 mV/second scan rates for half-cell CNF mat batteries, (d) schematic emphasizing the benefit of a 3-D mat for utilization of a macroscopically accessible active material.

In galvanostatic measurements (Fig. 5a), we compared discharge rates from C/10 to 10C ($C = 372 \text{ mAh/g}$) to assess the rate capability of the device (plots in Fig. 5b). At C/10 rates, we observed 2 V capacities measured to be 253 mAh/g. At high currents (10C, or 3.7 A/g), we still observed capacities of 49 mAh/g. Compared to the rate capability of graphite materials,²³ where the capacity drops to $\sim 150 \text{ mAh/g}$ at rates of 100 mA/g, our macroscopically thick mats exhibit $\sim 150 \text{ mAh/g}$ capacities at over 3.5X faster charging rates (1C), emphasizing greater rate capability compared to bulk carbons. Also emphasized from Fig. 4b are the near 100% Coulombic efficiencies measured in these devices over a period of cycling at 2 C for 150 cycles with $\sim 90\%$ capacity retention. This is comparable or better than previous studies on CNF electrodes, which often exhibit more than 10% capacity fade over 25-50 cycles.^{22, 23} CV scans (Fig 4c) further highlight the device rate capability based on measurements carried out at scan rates between 0.1 – 1 mV/second. In these curves the bulk insertion and de-insertion reactions correspond to the reversible formation of a conventional bulk compound resembling that of LiC_6 . Although the capacities are average, the CNF mats have been used as-is (i.e., not functionalized). The benefit of these CNF mats compared to bulk film electrodes, especially after functionalization with active material such as silicon³⁴, lies in the improved diffusion of Li through the 3-D millimeter thickness scale structure, which would enable most of the material to be active for storage unlike comparable millimeter-scale bulk carbon electrodes. To summarize, the fully accessible surface of the CNF mats, combined with their porous and conductive nature, make them a suitable freestanding architecture that could be functionalized (post-process) with high capacity anode materials for developing more efficient battery electrodes.

Conclusions

Whereas the delamination-based technique described has been applied to synthesize large CNF mats, it should be noted that the observations reported in this work are generally universal to CNTs that grow from solid substrates. It is known in such materials that catalyst-support layer interactions similarly dictate the growth properties observed, and thus we anticipate the results of this work to be transferable to CNTs. In this manner, the ability to utilize growth as a tool to nanomanufacture carbon nanostructured templates in one step, without additional transfer or binding post-processes, could enable the large-scale fabrication of new materials for applications such as electrochemical energy storage systems. In particular, we demonstrate a growth-to-applications route to

thick CNF freestanding materials that can serve as conductive, freestanding templates for novel functionalized electrodes.

Acknowledgements

Dr. Nessim and Efrat Shawat were partially supported the Israel National Research Center for Electrochemical Propulsion (INREP; I-CORE Program of the Planning and Budgeting Committee and The Israel Science Foundation 2797/11). Dr. Pint and Andrew Westover acknowledge support from NSF grant EPS 1004083. We thank Professor Doron Aurbach (Bar Ilan University) for useful discussions, Klimentiy Shimanovich (Bar Ilan University) for four-point probe measurements, Dr. Irena Gouzman and Kobi Carmiel for contact angle measurements, and Yana Miroshnikov (Bar Ilan University) for Raman measurements.

References

1. M. Chhowalla, K. B. K. Teo, C. Ducati, N. L. Rupesinghe, G. A. J. Amaratunga, A. C. Ferrari, D. Roy, J. Robertson and W. I. Milne, *J Appl Phys*, 2001, **90**, 5308-5317.
2. N. M. Rodriguez, *J. Mater. Res.*, 1993, **8**, 3233-3250.
3. K. P. De Jong and J. W. Geus, *Catalysis Reviews-Science and Engineering*, 2000, **42**, 481-510.
4. S. Motojima, M. Kawaguchi, K. Nozaki and H. Iwanaga, *Carbon*, 1991, **29**, 379-385.
5. Y. A. Kim, T. Hayashi, M. Endo, M. S. Dresselhaus and *Springer Handbook of Nanomaterials*, Springer, 2013.
6. M. Endo, Y. A. Kim, T. Hayashi, K. Nishimura, T. Matusita, K. Miyashita and M. S. Dresselhaus, *Carbon*, 2001, **39**, 1287-1297.
7. G. G. Tibbetts, M. L. Lake, K. L. Strong and B. P. Rice, *Compos. Sci. Technol.*, 2007, **67**, 1709-1718.
8. G. D. Nessim, *Nanoscale*, 2010, **2**, 1306-1323.
9. T. Yamada, T. Namai, K. Hata, D. N. Futaba, K. Mizuno, J. Fan, M. Yudasaka, M. Yumura and S. Iijima, *Nat Nanotechnol*, 2006, **1**, 131-136.
10. G. D. Nessim, M. Seita, K. P. O'Brien and S. A. Speakman, *Carbon*, 2010, **48**, 4519-4526.
11. D. S. Bethune, R. D. Johnson, J. R. Salem, M. S. Devries and C. S. Yannoni, *Nature*, 1993, **366**, 123-128.
12. R. L. Vander Wal, T. M. Ticich and V. E. Curtis, *Carbon*, 2001, **39**, 2277-2289.
13. A. Gohier, C. P. Ewels, T. M. Minea and M. A. Djouadi, *Carbon*, 2008, **46**, 1331-1338.
14. H. Cui, X. Yang, M. L. Simpson, D. H. Lowndes and M. Varela, *Appl. Phys. Lett.*, 2004, **84**, 4077.

15. A. Rothlisberger, M. Seita, A. Reiser, E. Shawat, R. Spolenak and G. D. Nessim, *Carbon*, 2013, **63**, 498-507.
16. G. D. Nessim, D. Acquaviva, M. Seita, K. P. O'Brien and C. V. Thompson, *Adv. Funct. Mater.*, 2010, **20**, 1306-1312.
17. C. L. Pint, N. T. Alvarez and R. H. Hauge, *Nano Res.*, 2009, **2**, 526-534.
18. Z. Yan, L. Ma, Y. Zhu, I. Lahiri, M. G. Hahm, Z. Liu, S. Yang, C. Xiang, W. Lu, Z. Peng, Z. Sun, C. Kittrell, J. Lou, W. Choi, P. M. Ajayan and J. M. Tour, *Acs Nano*, 2013, **7**, 58-64.
19. C. L. Pint, K. Takei, R. Kapadia, M. Zheng, A. C. Ford, J. Zhang, A. Jamshidi, R. Bardhan, J. J. Urban, M. Wu, J. W. Ager, M. M. Oye and A. Javey, *Adv. Energ. Mater.*, 2011, **1**, 1040-1045.
20. N. M. Rodriguez, M.-S. Kim and R. T. K. Baker, *J. Phys. Chem.*, 1994, **98**, 13108-13111.
21. M. D. Volder, S. Tawfick, S. J. Park, D. Copic, Z. Zhao, W. Lu and A. J. Hart, *Adv. Mater.*, 2010, **22**, 4384-4389.
22. L. Ji and X. Zhang, *Nanotechnol.*, 2009, **20**, 155705.
23. C. Kim, K. S. Yang, M. Kojima, K. Yoshida, Y. J. Kim, Y. A. Kim and M. Endo, *Adv. Funct. Mater.*, 2006, **16**, 2393-2397.
24. V. Subramanian, H. Zhu and B. Wei, *J. Phys. Chem. B*, 2006, **110**, 7178-7183.
25. P. Meduri, J. H. Kim, H. B. Russell, J. Jasinski, G. U. Sumanasekera and M. K. Sunkara, *J. Phys. Chem. C*, 2010, **114**, 10621-10627.
26. G. Zou, D. Zhang, C. Dong, H. Li, K. Xiong, L. Fei and Y. Qian, *Carbon*, 2006, **44**, 828-832.
27. G. D. Nessim, A. Al-Obeidi, H. Grisaru, E. S. Polsen, C. R. Oliver, T. Zimrin, A. J. Hart, D. Aurbach and C. V. Thompson, *Carbon*, 2012, **50**, 4002-4009.
28. G. D. Nessim, *Nano Lett*, 2009, **9**, 3398.
29. G. D. Nessim, M. Seita, D. L. Plata, K. P. O'Brien, A. J. Hart, E. R. Meshot, C. M. Reddy, P. M. Gschwend and C. V. Thompson, *Carbon*, 2011, **49**, 804-810.
30. E. R. Meshot, *Acs Nano*, 2009, **3**, 2477.
31. M. Maciejewski, *Pure and Applied Chemistry*, 1995, **67**, 1879.
32. H. Okamoto, *Desk handbook : phase diagrams for binary alloys, ASM International, Materials Park*, 2010.
33. L. Ji, Z. Lin, M. Alcoutabi and X. Zhang, *Energy Environ. Sci.*, 2011, **4**, 2682-2699.
34. R. Teki, M. K. Datta, R. Krishnan, T. C. Parker, T.-M. Lu, P. N. Kumta and N. Koratkar, *Small*, 2009, **5**, 2236-2242.